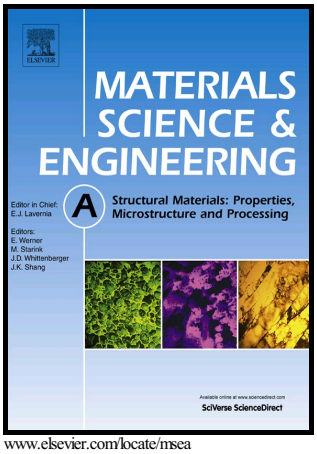

www.elsevier.com/locate/msea

Predictive models for physical and mechanical properties of 316L stainless steel produced by selective laser melting

G. Miranda, S. Faria, F. Bartolomeu, E. Pinto, S. Madeira, A. Mateus, P. Carreira, N. Alves, F.S. Silva, O. Carvalho

PII: S0921-5093(16)30027-2
DOI: http://dx.doi.org/10.1016/j.msea.2016.01.028
Reference: MSA33215

To appear in: *Materials Science & Engineering A*

Received date: 27 December 2015
Revised date: 7 January 2016
Accepted date: 8 January 2016

Cite this article as: G. Miranda, S. Faria, F. Bartolomeu, E. Pinto, S. Madeira, A Mateus, P. Carreira, N. Alves, F.S. Silva and O. Carvalho, Predictive models for physical and mechanical properties of 316L stainless steel produced by selectiv laser melting, *Materials Science & Engineering A* http://dx.doi.org/10.1016/j.msea.2016.01.028

Predictive models for physical and mechanical properties of 316L stainless steel produced by selective laser melting

G. Miranda[a*], S. Faria[b], F. Bartolomeu[a], E. Pinto[c], S. Madeira[a], A. Mateus[c], P. Carreira[c], N. Alves[c], F. S. Silva[a], O. Carvalho[a]

[a] Center for Micro-Electro Mechanical Systems (CMEMS)
University of Minho, Campus de Azurém, 4800-058 Guimarães – Portugal

[b] CMAT - Center of Mathematics, Department Mathematics and Applications, University of Minho, Portugal

[c] Centre for Rapid and Sustainable Product Development (CDRSP)
Polytechnic Institute of Leiria, Rua General Norton de Matos, Apartado 4133, 2411-901 Leiria - Portugal

*Corresponding author – G. Miranda (gmiranda@dem.uminho.pt)

Abstract

Selective Laser Melting (SLM) processing parameters are known to greatly influence 316L stainless steel final properties. A simple energy density calculation is insufficient for explaining mechanical and physical properties as well as microstructural characteristics, which are known to significantly influence these parts performance. In fact, parts produced by using different combinations of processing parameters, even presenting similar energy density, can display different properties. Thus, it is necessary to assess their influence as isolated parameters but also their interactions.

This work presents a study on the influence of several SLM processing parameters (laser power, scanning speed and scanning spacing) on density, hardness and shear strength of 316L stainless steel. The influence of these processing parameters on the abovementioned properties is assessed by using statistical analysis. In order to find the significant main factors and their interactions, analysis of variance (ANOVA) is used. Furthermore, in order to assess the effect of the part building orientation, two different building strategies were tested. The influence of these processing parameters on shear strength, hardness and density were assessed for the two building strategies, thus resulting six different models that can be used as predictive design tools. The microstructures experimentally obtained were analyzed, discussed and correlated with the obtained models.

Keywords: Selective Laser Melting; 316L stainless steel; Predictive models; Density; Mechanical properties.

1. Introduction

Selective laser melting/sintering (SLM/SLS) are additive manufacturing (AM) processes that apply laser energy to powder beds in order to melt/sinter metals, ceramics or polymers. Starting with a 3-D CAD drawing of the part, the process proceeds by laser melting or sintering sequential powders layers, thus obtaining the cross-sections of the final part. This technology brings an extraordinary freedom when regarding geometry and materials design, suited for producing parts with local functional requirements.

SLM/SLS parts properties are greatly influenced by the processing parameters like laser power, scan spacing and speed, among other [1, 2]. Several studies have been made regarding SLM processing parameters influence on the final parts microstructural and mechanical properties, for different materials [3 – 9]. Regarding stainless steel there are some studies that assess optimal SLM/SLS parameters. K. Antony et al. [10] performed a numerical and experimental investigation on laser melting of 316L powder, assessing the influence of laser power, scanning speed and beam size on geometric characteristics of the melt zone and ball formation. C. Yan et al. [11] investigated the manufacturability and performance of stainless steel cellular lattice structures fabricated via SLM. C. Yan study tested the influence of a single set of processing conditions on the compression modulus and yield strength. A. Riemer et al. [12] analyzed the fatigue crack growth behavior in 316L manufactured by SLM. R. Li et al. [13] studied the densification process of 316L during SLM process by varying four processing parameters: laser power, scanning speed, hatch spacing and layer thickness.

More focused on biomedical applications there are some studies regarding stainless steel and hydroxyapatite (HAP) composites processed by SLM [14, 15]. L. Hao et al. [14] identified the optimum SLM parameters (laser power, scanning speed, scanning procedure and scan line spacing) for a stainless steel and HAP composite, analyzing the tensile strength, hardness, density and microstructure. Q. Wei et al. [15] have identified the effect of stainless steel/HAP ratios and laser scanning speeds on cracks and pores of composites fabricated by SLM. In this study laser power, layer thickness and scanning space were maintained constants.

Predictive models are powerful tools for use on numerous fields [16, 17] and can be developed using several strategies [18, 19]. In this work, a wide approach on the influence of several processing parameters, namely laser power, scanning speed and distance between scanning lines on the density, hardness and shear strength of 316L stainless steel produced by selective laser melting is performed. The influence of these processing parameters on the abovementioned properties is modelled by several proposed equations. In order to assess the influence of orientation, two building orientations – named horizontal and vertical were investigated when regarding the influence of processing parameters on shear

strength, hardness and density. A study on the microstructure of the 316L stainless steel samples was performed and correlated with the obtained properties.

2. Experimental procedure

2.1. Material

316L stainless steel specimens were produced by using a SLM/SLS equipment from SLM Solutions (model 125 HL). The main characteristics of this equipment are presented on Table 1.

Table 1. SLM solutions equipment (model 125 HL) characteristics.

Laser type	Yb-Faser-Laser
Effective build volume [mm x mm x mm]	125 x 125 x 125
Laser power [W]	40 - 100
Scanning speed [mm/s]	100 - 2000
Layer thickness [µm]	20 - 40
Distance between scanning lines [mm]	0.07 - 0.15
Laser spot [µm]	87
Inert gas (Ar/N_2) flow during production [L/min]	0.5
Inert gas (Ar/N_2) flow during the filling of the chamber [L/min]	10

The 316L stainless steel powder was purchased from the manufacturer of the equipment, which provided the powder composition as shown on Table 2. Figure 1 shows the spherical powder, while Figure 2 shows the powder size distribution.

Table 2. 316L stainless steel powder composition.

Element	**Fe**	**Cr**	**Ni**	**Mo**	**Mn**	**Si**
wt. %	balance	16.97	12.28	2.39	1.24	0.46

O	**Cu**	**N**	**S**	**P**	**C**
0.05	0.01	0.01	0.006	<0.005	0.03

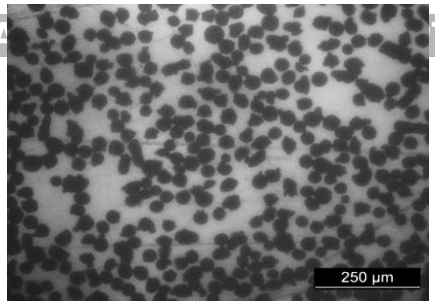

Figure 1. 316L stainless steel powder.

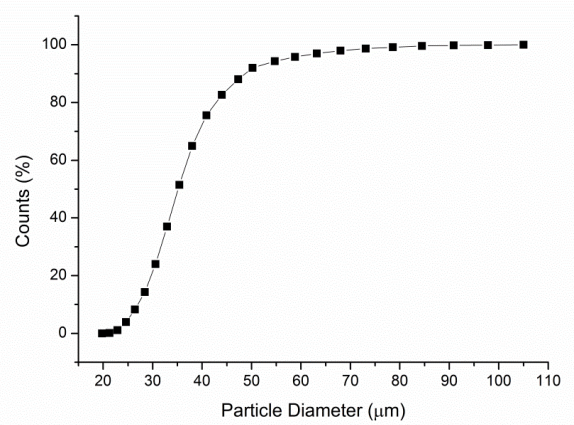

Figure 2. 316L stainless steel powder size distribution.

2.2. Processing parameters selection and specimens production

The energy density [J/mm^3] during SLM/SLS process can be calculated by using the following equation [20]:

$$E = \frac{P}{v \times d \times e}$$

where P represents the laser power [W]; v the scanning speed [mm/s]; d the distance between scanning lines and e the layer thickness.

In this study, e was maintained constant (0.03 mm), while the remaining parameters varied as shown on Table 3. Samples were produced with an energy density ranging from 31.7 to 79.9 J/mm^3 (once the equipment manufacturer recommends the use of an energy density between 50 and 80 J/mm^3).

The platform temperature was maintained constant at 200ºC for all specimens produced. The variation on the processing parameters (see Table 3) was performed in order to assess the influence of the following parameters: laser power, scan speed and scan spacing on the obtained specimen's shear strength, hardness and density. For each condition (1 to 48) three specimens were produced and characterized. The produced specimens were cylindrical with an average diameter of 6.1 mm and average height of 5.5 mm.

Following the plan of experiments indicated on Table 3 (conditions 1 to 48), two building strategies were used, thus resulting in two types of specimens produced, named horizontal e vertically built, both represented on Figure 3.

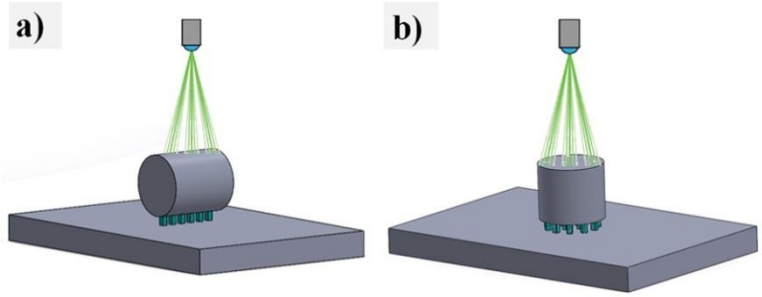

Figure 3. Specimens building strategy: a) horizontal and b) vertical.

Table 3. Plan of experiments for specimen's production.

	A	B	C			A	B	C	
Exp. number	**Laser power [W]**	**Scan speed [mm/s]**	**Scan spacing [mm]**	**Energy density [J/mm^3]**	**Exp. number**	**Laser power [W]**	**Scan speed [mm/s]**	**Scan spacing [mm]**	**Energy density [J/mm^3]**
1	100	417	0.15	53.3	25	50	400	0.07	59.5
2	100	417	0.14	57.1	26	50	400	0.08	52.1
3	100	417	0.12	66.6	27	50	400	0.09	46.3
4	100	417	0.11	72.7	28	50	400	0.10	41.7
5	100	733	0.08	56.8	29	50	400	0.11	37.9
6	100	733	0.07	65.0	30	60	300	0.09	74.1
7	90	417	0.14	51.4	31	60	400	0.09	55.6
8	90	417	0.12	60.0	32	60	500	0.09	44.4
9	90	417	0.11	65.4	33	60	600	0.09	37.0
10	90	417	0.10	71.9	34	60	700	0.09	31.7
11	90	733	0.07	58.5	35	70	550	0.07	60.6
12	80	417	0.12	53.3	36	70	550	0.08	53.0
13	80	417	0.11	58.1	37	70	550	0.09	47.1
14	80	417	0.10	63.9	38	70	550	0.10	42.4
15	80	417	0.08	79.9	39	70	550	0.11	38.6
16	80	733	0.07	52.0	40	80	800	0.09	37.0
17	70	417	0.11	50.9	41	80	400	0.09	74.1
18	70	417	0.10	56.0	42	80	700	0.09	42.3
19	70	417	0.08	69.9	43	80	500	0.09	59.3
20	70	417	0.07	79.9	44	80	600	0.09	49.4
21	60	417	0.10	48.0	45	90	1250	0.07	34.3
22	60	417	0.08	60.0	46	90	700	0.12	35.7
23	60	417	0.07	68.5	47	100	1250	0.07	3.1
24	50	417	0.07	57.1	48	100	700	0.12	39.7

2.3. Microstructure analysis and density measurement

After processing, the specimens were polished in order to acquire optical microscope images. The specimen's density was obtained by image analysis, applying a threshold filter in order to assess the porosity percentage and the density (for each type of specimen three images were analyzed). An etching solution ("aqua regia" (75% HNO_3 and 25% HCl)) was used to reveal the microstructure of all the produced specimens.

Both types of specimens (horizontal and vertically built) were polished in the circular top/bottom faces. For horizontal specimens, images acquired in this face will allow the analysis of the specimen growing direction, observing the powder layers thickness and the laser spot (diameter and depth) (see Figures 17, 18 and 19). For vertical specimens, the images acquired in this face will reveal the laser spot path and the scan spacing (see Figures 20, 21 and 22).

2.4. Shear strength and hardness measurement

Hardness measurements were conducted using an EMCO-TEST, DuraScan model hardness tester, with a dwell time of 15 s under a load of 3kgf, to obtain Vickers Hardness. Three indentations were made in each sample.

Shear tests were performed at room temperature (≈ 23ºC), with a crosshead speed of 0.02 mm/s, in a servohydraulic machine (Instron 8874 MA. USA), equipped with a 25 kN capacity load cell. Tests were performed using a custom-made stainless steel apparatus (shown in Figure 4 a)) with a sliding part equipped with a cutting tool. A compressive force was applied in the sliding part to promote fracture due to shear loading (Figure 4 b)). The cylindrical specimens were positioned in order to promote loading through the longitudinal plan.

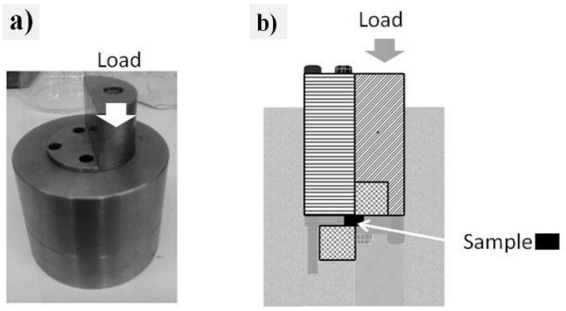

Figure 4. (a) Custom-made apparatus used to perform shear tests and (b) schematic illustration of the test [21].

2.5. Statistical analysis

Response surface methodology (RSM) is a statistical method used for experimental modeling and analyzing the relationship between the input and response variables. Besides, RSM also reduces the number of required experimental runs to generate statistically validated results.

The mathematical models for the desired responses as a function of selected variables were developed by applying the multiple regression analysis on the experimental data. The general quadratic equation model is stated by:

$$Y_k = b_0 + \sum_{i=1}^{3} b_i X_i + \sum_{i=1}^{3} b_{ii} {X_i}^2 + \sum_{i=1}^{2} \sum_{j>1}^{3} b_{ij} X_i X_j + \varepsilon$$

where Y_k represents the response variables (dependent variables), b_0 is the constant, ε is the residual (error) term, b_i is the linear coefficient, b_{ii} is the quadratic coefficient, b_{ij} is the interaction coefficient and X_i, X_j are dimensionless coded independent variables.

For finding the significant factors (main and interactions) analysis of variance (ANOVA) has been used. The quality of developed model was determined by the coefficients of determination (R^2). These R^2 coefficients have values between 0 and 1. A test for lack-of fit indicating the significance of the replicate error in comparison to the model dependent error was performed. Insignificant lack-of-fit is desired as significant lack-of-fit indicates that there might be contributions in the regressor–response relationship that are not accounted for by the model.

Further, adequate precision was used to measure the signal to noise ratio. A ratio greater than 4 is desirable. In addition to the above, the adequacy of the model is also investigated by the examination of residuals. The residuals are examined using the normal probability plots of the residuals and the plots of the residuals versus the predicted response. If the model is adequate, the points on the normal probability plots of the residuals should form a straight line. On the other hand the plots of the residuals versus the predicted response should contain no obvious patterns.

3. Results and discussion

In this study a total of 48 experiments were conducted for each growing direction, varying three independent variables, as indicated on Table 3. For these experiments, three dependent variables were assessed: shear strength, hardness and density.

3.1. Statistical analysis of results

Regression models were developed using the input and output data. Analysis of variance (ANOVA) for second-order regression models were obtained for shear strength, hardness and density. This analysis estimated the effect of significant variables and moreover their interaction on the abovementioned properties of horizontal e vertical sintered specimens.

These models allow assessing the significance of SLM process variables on the shear strength, hardness and density of these parts and demonstrate that not only the analysis of the energy density is required when selecting the best processing conditions, but a more thorough analysis on the several processing parameters is necessary. In this sense, these models allow to determine the optimal working conditions for achieving parts with higher properties.

Horizontally built specimens

Starting by horizontally built parts (Figure 3 a)), the model for shear strength that was shown to fit the data appropriately is a two factor interaction model, as follows:

$$Shear\ Strength = 539.725 + 3.752\mathrm{A} - 9.311\mathrm{B} - 2.613\mathrm{C} - 2.477\mathrm{AC}$$

Statistical results of the ANOVA analysis for shear strength are found on Table 4. The probability values (<0.05) found for A, B, C, and AC shear strength model terms indicate that these are the significant model terms for this case.

Table 4. Summary of ANOVA and regression analysis for shear strength (for horizontally built specimens).

Model terms	Sum of Squares	Degree of freedom	Mean Square	F value	P-value
Model	2097.307	4	524.327	8.487	< 0.001
A	270.792	1	270.792	4.383	0.048
B	412.253	1	412.253	6.673	0.017
C	245.640	1	245.640	3.976	0.049
AC	1314.380	1	1314.380	21.275	< 0.001
Residuals	1359.080	22	61.780		
Lack of fit	909.270	17	53.490	0.595	0.807
Pure error	449.810	5	89.960		
Cor. total	3456.387	26			

Multiple R^2: 0.607

Adjusted R^2: 0.535

Predicted R^2: 0.417

Adequate precision: 8.990

The obtained shear strength model F value of 8.487 indicates that the model is significant. The lack-of-fit F value of 0.595 indicates that lack of fit is non-significant, as it is desirable. All the adequacy measures for the model, such as R^2 (0.607), adjusted R^2 (0.535) and predicted R^2 (0.417) are in good agreement, which provide an adequate signal and confirms that the predicted model for shear strength [MPa] can be employed.

As given in Table 4, adequate precision value for the model equation was 8.990. It was concluded that the signal was adequate and that the model was able to give reasonable performance according to the prediction.

The normal probability plots of the residuals and the plots of the residuals versus the predicted response for shear strength [MPa] are shown in Figures 5 and 6, respectively. A check on the plot in Figure 5 revealed that the residuals generally fall on a straight line implying that the errors are distributed normally. Also Figure 6 revealed that they have no obvious pattern and unusual structure. This implies that the models proposed are adequate and there is no reason to suspect any violation of the independence or constant variance assumption.

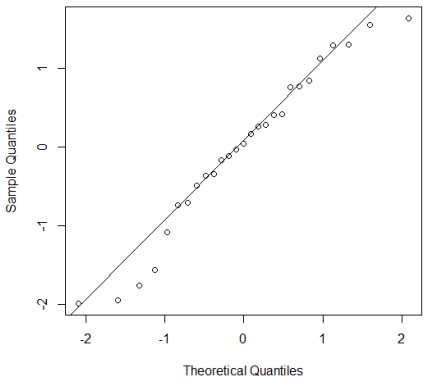

Figure 5. Normal probability plot of the residuals for shear strength data.

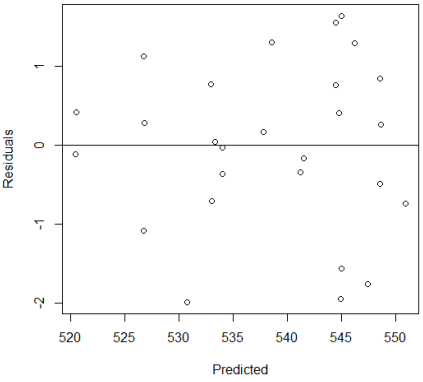

Figure 6. Plot of residuals vs. predicted response for shear strength data.

The obtained model for predicting hardness is also a two factor interaction model:

$$Hardness = 217.717 + 4.967\mathrm{A} - 7.147\mathrm{B} - 3.267\mathrm{C} - 1.336\mathrm{AC}$$

Statistical results of the ANOVA for hardness are found on Table 5. Probability values (<0.05) for A, B, C and AC model terms indicate that these are the significant model terms for the hardness model.

Regarding hardness model, an F value of 3.196 indicates that the model is significant and a lack-of-fit F value of 0.430 indicates that the lack of fit is non-significant. Additionally, R^2 (0.368), adjusted

R^2 (0.253) and predicted R^2 (0.0890) are in good agreement, which provide an adequate signal and confirms that the predicted model for hardness [HV] can be employed.

Table 5. Summary of ANOVA and regression analysis for hardness (for horizontally built specimens).

Model terms	Sum of Squares	Degree of freedom	Mean Square	F-value	P-value
Model	683.561	4	170.890	3.196	0.033
A	450.241	1	450.241	8.421	0.008
B	264.448	1	264.448	4.946	0.037
C	346.275	1	346.275	6.476	0.018
AC	318.652	1	318.652	5.960	0.023
Residuals	1176.290	22	53.470		
Lack of fit	628.620	16	39.290	0.430	0.917
Pure error	547.670	6	91.280		
Cor. total	1859.851	26			
				Multiple R^2: 0.368	
				Adjusted R^2: 0.253	
				Predicted R^2: 0.089	
				Adequate precision: 6.180	

For hardness model, the normal probability plots of the residuals (Figure 7) show that the errors are distributed normally and the plots of the residuals versus the predicted response (Figure 8) show no obvious pattern and unusual structure implying that this model is adequate.

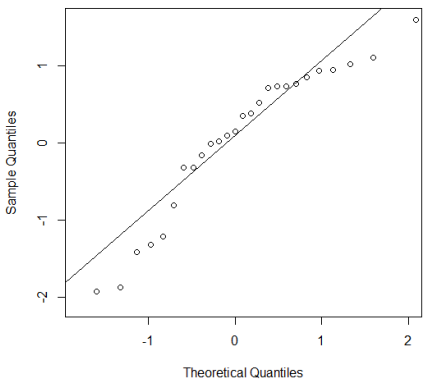

Figure 7. Normal probability plot of the residuals for hardness data.

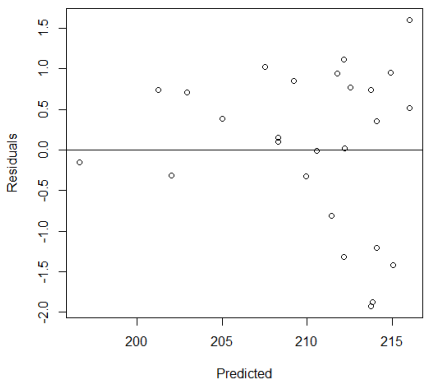

Figure 8. Plot of residuals vs. predicted response for hardness data.

Regarding density, a two factor interaction model is proposed as:

$$Density = 99.734 + 0.227\mathrm{A} - 1.136\mathrm{B} - 0.481\mathrm{C} - 0.521\mathrm{AB} - 0.222\mathrm{AC}$$

Statistical results of the ANOVA are shown on Table 6 and probability values (<0.05) for A, B, C, AB and AC model terms indicate that these are the significant model terms for the density model.

Density model F value of 15.840 indicates that the model is significant and the lack-of-fit F value of 0.426 indicates that lack of fit is non-significant. For this model, R^2 (0.783), adjusted R^2 (0.733) and predicted R^2 (0.630) are in good agreement.

Table 6. Summary of ANOVA and regression analysis for density (for horizontally built specimens).

Model terms	Sum of Squares	Degree of freedom	Mean Square	F-value	P-value
Model	11.012	5	2.753	15.840	< 0.001
A	0.466	1	0.466	2.688	0.116
B	3.762	1	3.762	21.646	< 0.001
C	6.480	1	6.480	37.283	< 0.001
AB	2.577	1	2.577	14.830	< 0.001
AC	8.679	1	8.679	49.938	< 0.001
Residuals	3.824	22	0.174		
Lack of fit	2.033	16	0.127	0.426	0.919
Pure error	1.791	6	0.298		
Cor. total	13.045	27			
				Multiple R^2: 0.783	
				Adjusted R^2: 0.733	
				Predicted R^2: 0.630	
				Adequate precision: 16.068	

For density model, the normal probability plots of the residuals (Figure 9) show that the errors are distributed normally and the plots of the residuals versus the predicted response (Figure10) show no obvious pattern and unusual structure implying that this model is adequate.

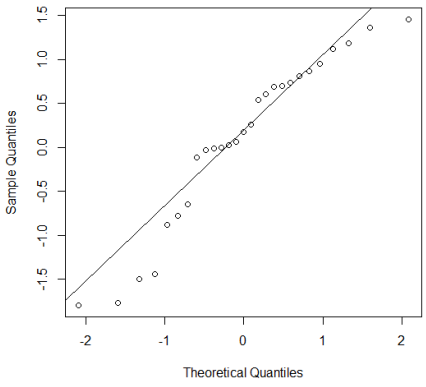

Figure 9. Normal probability plot of the residuals for density data.

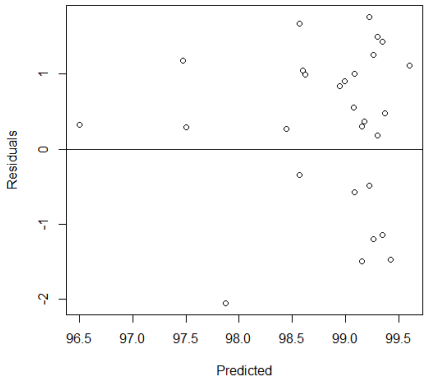

Figure 10. Plot of residuals vs. predicted response for density data.

Vertically built specimens

Regarding vertically built specimens (Figure 3 b)), the model for shear strength that was shown to fit the data appropriately is a quadratic model:

$$Shear\ Strength = 529.103 + 85.460\mathrm{A} - 28.715\mathrm{B} - 23.314\mathrm{C} + 31.132\mathrm{AB} - 47.540A^2 - 4.071B^2$$

The statistical results of the ANOVA are shown on Table 7. Probability values (<0.05) for A, B, C, AB, A^2 and B^2 model terms indicate that these are the significant model terms for shear strength model.

The obtained shear strength model F value of 20.120 indicates that the model is significant. The lack-of-fit F value of 0.729 indicates that lack of fit is non-significant. The value of determination coefficient R^2 (0.765) indicates the goodness of fit for the used model (see Table 7). The predicted R^2 (0.669) has an acceptable agreement with the adjusted R^2 (0.727) providing an adequate signal and confirming that the predicted model for shear strength [MPa] can be employed.

As given in Table 7, adequate precision value for the model equation was 17.073. It was concluded that the signal was adequate and that the model was able to give reasonable performance according to the prediction.

Table 7. Summary of ANOVA and regression analysis for shear strength (for vertically built specimens).

Model terms	Sum of Squares	Degree of freedom	Mean Square	F-value	P-value
Model	447267.60	6	74544.60	20.120	< 0.001
A	282957.80	1	282957.80	76.372	< 0.001
B	139586.00	1	139586.00	37.675	< 0.001
C	22339.22	1	22339.20	6.029	0.019
AB	152060.50	1	152060.50	41.042	< 0.001
A^2	137235.50	1	137235.50	37.041	< 0.001
B^2	88254.05	1	88254.10	23.820	< 0.001
Residuals	137095	37	3705		
Lack of fit	52447	17	3085	0.729	0.743
Pure error	84648	20	4232		
Cor. total	584362.6	43			
				Multiple R^2: 0.765	
				Adjusted R^2: 0.727	
				Predicted R^2: 0.669	
				Adequate precision: 17.073	

For the shear strength model, the normal probability plots of the residuals (Figure 11) revealed that the residuals generally fall on a straight line implying that the errors are distributed normally. The plots of the residuals versus the predicted response (Figure 12) revealed no obvious pattern and unusual structure, implying that the proposed model is adequate and there is no reason to suspect any violation of the independence or constant variance assumption.

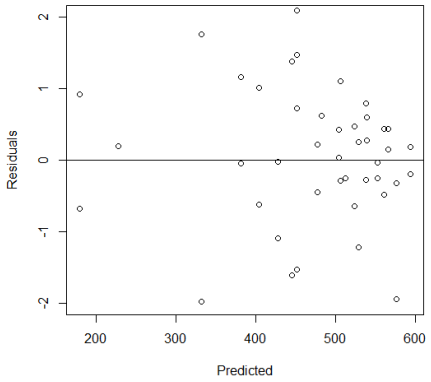

Figure 11. Normal probability plot of the residuals for shear strength data.

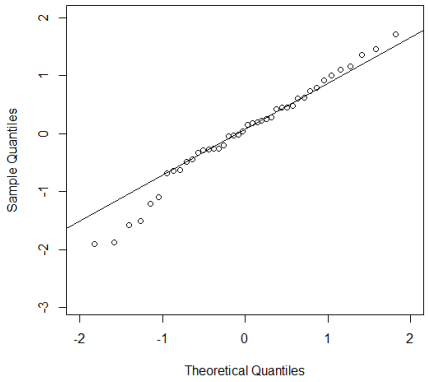

Figure 12. Plot of residuals vs. predicted response for shear strength data.

The obtained model for predicting hardness is a two factor interaction model:

$$Hardness = 182.784 + 17.283\mathrm{A} - 4.850\mathrm{B} - 4.240\mathrm{C} - 0.726\mathrm{AB} - 5.499\mathrm{AC}$$

Table 8. Summary of ANOVA and regression analysis for hardness (for vertically built specimens).

Model terms	Sum of Squares	Degree of freedom	Mean Square	F-value	P-value
Model	16430.26	5	2738.38	13.140	< 0.001
A	9839.84	1	9839.84	47.216	< 0.001
B	4878.06	1	4878.06	23.407	< 0.001
C	1069.23	1	1069.23	5.131	0.029
AB	900.41	1	900.41	4.321	0.044
AC	7560.53	1	7560.53	36.279	< 0.001
Residuals	8127.70	39	208.40		
Lack of fit	4463.70	18	248.00	1.421	0.219
Pure error	3663.90	21	174.50		
Cor. total	24557.95	44			
				Multiple R^2: 0.627	
				Adjusted R^2: 0.580	
				Predicted R^2: 0.551	
				Adequate precision: 13.640	

Hardness model F value (13.140) indicates that the model is significant and the value of determination coefficient R^2 (0.627) indicates the goodness of fit for this model (see Table 8). The predicted R^2 (0.551) was in acceptable agreement with the adjusted R^2 (0.580) confirming that the predicted model for hardness [HV] can be employed.

As given in Table 8, adequate precision value for the model equation was 13.640. It was concluded that the signal was adequate and that the model was able to give reasonable performance according to the prediction. For hardness model, the normal probability plots of the residuals (Figure 13) show that the errors are distributed normally and the plots of the residuals versus the predicted response (Figure 14) show no obvious pattern and unusual structure implying that this model is adequate.

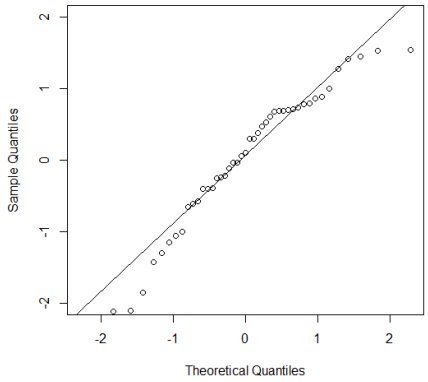

Figure 13. Normal probability plot of the residuals for hardness data.

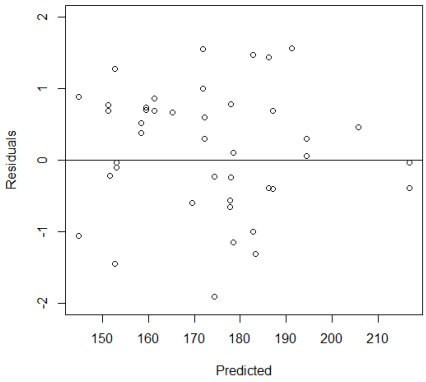

Figure 14. Plot of residuals vs. predicted response for hardness data.

Regarding density, a quadratic model is proposed as:

$$\text{Density} = 94.474 + 7.790A - 2.265B - 3.227C - 3.105AB - 2.859AC - 5.017A^2 - 0.409B^2 - 1.763C^2$$

Density model F value (21.860) indicates that the model is significant and the lack-of-fit F value of 0.616 indicates that lack of fit is non-significant. The value of determination coefficient R^2 (0.841) indicates the goodness of fit for the used model (Table 9). The predicted R^2 value of 0.717 was in acceptable agreement with the adjusted R^2 value confirming that the predicted model for density [%] can be employed.

As given in Table 9, adequate precision value for the model equation was 17.040. It was concluded that the signal was adequate and that the model was able to give reasonable performance according to the prediction.

Regarding density model, the normal probability plots of the residuals (Figure 15) show that the errors are distributed normally and the plots of the residuals versus the predicted response (Figure 16) show no obvious pattern and unusual structure implying that this model is adequate.

Table 9. Summary of ANOVA and regression analysis for density (for vertically built specimens).

Model terms	Sum of Squares	Degree of freedom	Mean Square	F-value	P-value
Model	4334.838	8	722.473	21.860	< 0.001
A	1840.716	1	1840.716	55.695	< 0.001
B	818.600	1	818.600	24.769	< 0.001
C	399.076	1	399.076	12.075	0.001
AB	1438.873	1	1438.873	43.536	< 0.001
AC	605.876	1	605.876	18.332	< 0.001
A^2	1015.053	1	1015.053	30.713	< 0.001
B^2	826.184	1	826.184	24.998	< 0.001
C^2	315.483	1	315.483	9.546	0.004
Residuals	1090.7	33	33.05		
Lack of fit	370.0	15	24.67	0.616	0.826
Pure error	720.7	18	40.04		
Cor. total	5425.538	41			
				Multiple R^2: 0.841	
				Adjusted R^2: 0.803	
				Predicted R^2: 0.717	
				Adequate precision: 17.040	

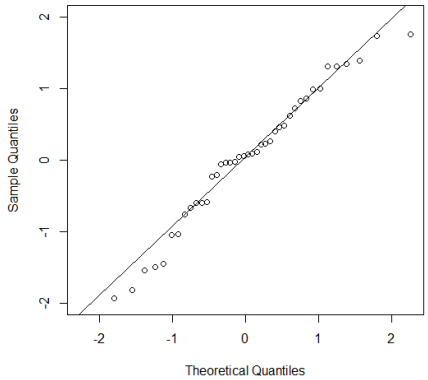

Figure 15. Normal probability plot of the residuals for density data.

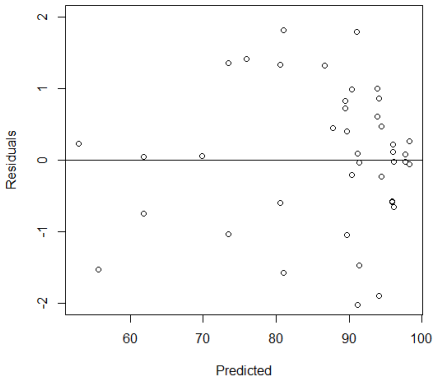

Figure 16. Plot of residuals vs. predicted response for density data.

In the following sections the effect of the processing parameters (laser power, scan speed and scan spacing) on shear strength, hardness and density will be addressed, as regarding their isolated influence (section 3.2.) as well as their interaction effect (section 3.3.). This discussion is made by analyzing the

developed models and the correspondent microstructures obtained. Additionally, the 3D response surface plots on a given response variable between two independent variables that are interacting are also analyzed.

3.2. Single parameters effect on shear strength, hardness and density

Horizontally built specimens

The three developed models for horizontally built specimens show that laser power, scan speed and scan spacing have a significant effect on shear strength, hardness and density.

At this point it is worth to mention that regarding horizontally built specimens, the images acquired exhibit the specimen growing direction, being observable the powder layers thickness and the laser spot diameter.

Regarding laser power (A), all models showed that by increasing power, for the tested power intervals, a higher shear strength, hardness and density are achieved. These results are correlated with the higher densification level and residual porosity progressive elimination, thus resulting in higher mechanical properties. These results are in accordance with Li et al. [13] and Hao et al. [14] results and are clear when observing Figures 17 a) and b), both obtained with the same scan speed and scan spacing, but differing in the laser power used (90 W and 60 W).

Figure 17 shows the powder layer being sequentially densified, however in Figure 17 b), due to a lower laser power, lower energy density is applied, therefore leading to consolidation defects (voids) between adjacent lines where the laser passed. In this sense, Figure 17 shows that when using lower laser power, higher porosity is present. On the other hand, when raising the laser power to 90W (Figure 17 a)), a structure totally absent of porosity is attained, thus leading to higher mechanical properties and density.

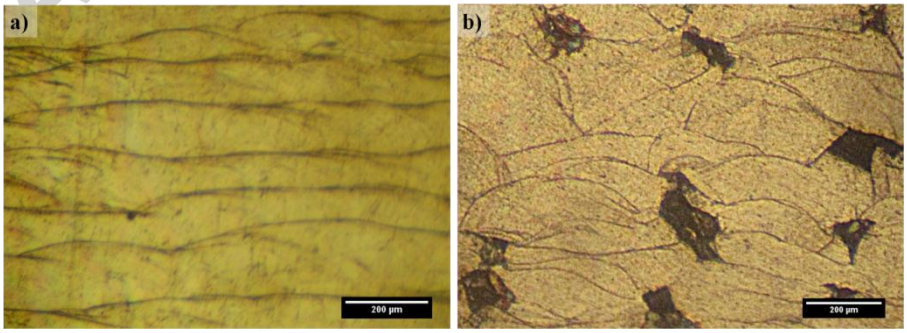

Figure 17. Horizontally built specimens from experiment number: a) 10 (90 W) and b) 21 (60 W).

Concerning scan speed (B), an opposite influence is observed, once by increasing speed, lower values for shear strength, hardness and density are attained. These results can be explained by the lower energy density delivered per second in a designated area, when the laser speed is increased. When analyzing Figure 18 it is visible that specimens produced with higher speed (Figure 18 b)) presented more consolidation defects than the one produced with lower speed (Figure 18 a)).

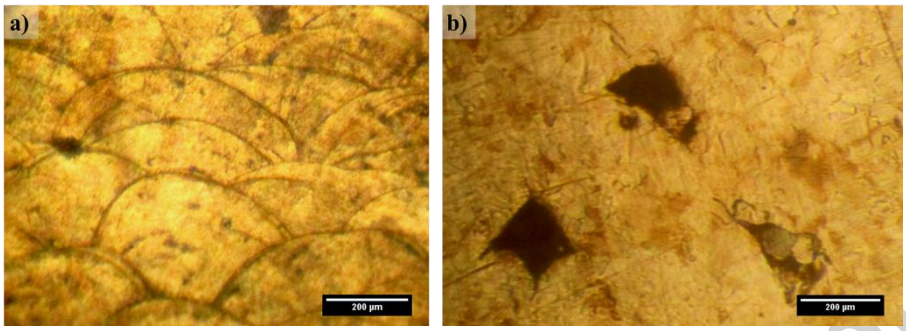

Figure 18. Horizontally built specimens from experiment number: a) 8 (417 mm/s) and b) 46 (700 mm/s).

Finally, regarding scan spacing (C), a similar trend than the one observed for laser speed is obtained, with higher spacing leading to lower values for shear strength, hardness and density. Higher scan spacing's can lead to poor sintering of adjacent regions of powder, not assuring a continuous bond between the consecutive lines of powders. This outcome leads to lower density and consequently lower mechanical properties.

By observing Figures 19 it is possible to verify some sintering defects on Figure 19 a) that corresponds to higher scan spacing (0.12 mm) than Figure 19 b). On the other hand, on Figure 19 b), obtained with 0.08 mm of scan spacing, no observable sintering flaws were detected.

Furthermore, the microstructure is also influenced by the scan spacing, with coarser structures being obtained when using higher scan spacing values (Figure 19 a)). This aspect can also be accountable for lowering the mechanical properties of the specimens produced with higher spacing.

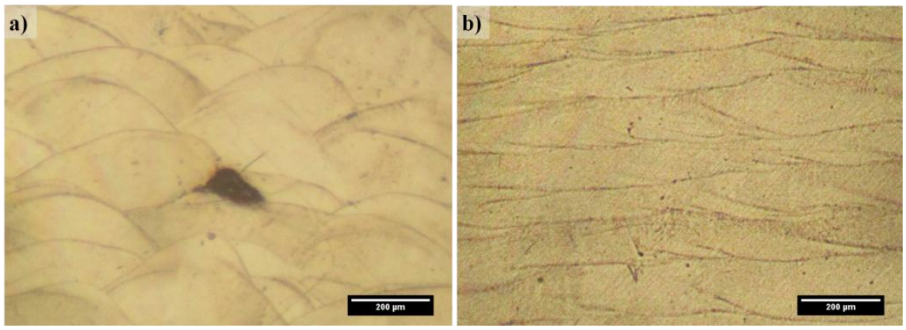

Figure 19. Horizontally built specimens from experiment number: a) 12 (0.12 mm) and b) 15 (0.08 mm).

An interesting observation is that, by analyzing the micrographs on Figures 18 and 19, speed seems to have a more pronounced influence than spacing, by influencing the specimen's consolidation. This fact is also verified when analyzing the models for hardness, shear strength and density for horizontally built parts, once the coefficients for speed present higher absolute values than that of spacing.

Figures 17 to 19 show that the molten material wet the underlying substrate (no balling effect occurred between subsequent layers of powders), a fundamental aspect when producing these materials by SLM, once it can lead to lower density, as reported by Kruth et al. [7] and consequently to lower mechanical properties.

Vertically built specimens

The three developed models for vertically built specimens show that laser power, scan speed and scan spacing have a significant effect on shear strength, hardness and density.

Regarding laser power (A), all models showed that by increasing power, a higher shear strength, hardness and density are achieved. Similarly to horizontally built specimens, these results are correlated with the higher densification level and residual porosity progressive elimination, thus resulting in higher mechanical properties. These findings are verifiable when analyzing Figure 20 b) where a high degree of porosity is found for the lower laser power used (60 W), unlike Figure 20 a) where a full densification is attained with the use of 90W (these specimens differ exclusively on the laser power, once they were produced with the same scan speed and spacing).

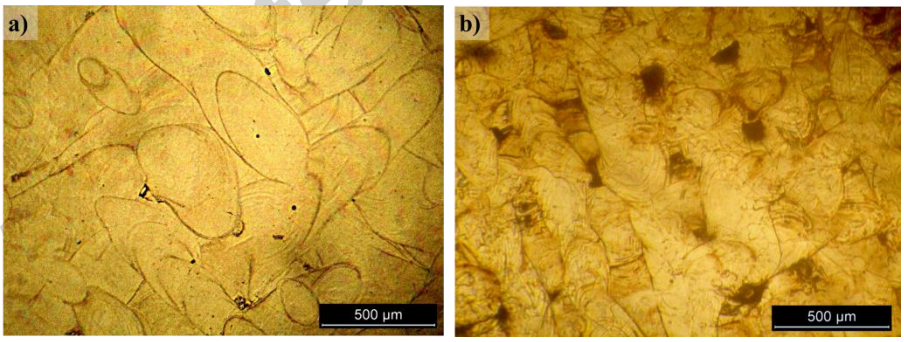

Figure 20. Vertically built specimens from experiment number: a) 10 (90 W) and b) 21 (60 W).

As for scan speed (B) as well as for scan spacing (C) an opposite influence is observed, once by increasing speed or spacing, lower values for shear strength, hardness and density are attained. Regarding scan speed, when this parameter is increased a lower energy density is delivered per second in a designated area, thus leading to lower consolidation and possible occurrence of consolidation defects (as

seen in Figure 21 b), representing a specimen processed using 700 mm/s, where there is a high prevalence of porosity, unlike Figure 21 a), representing a specimen processed using 417 mm/s).

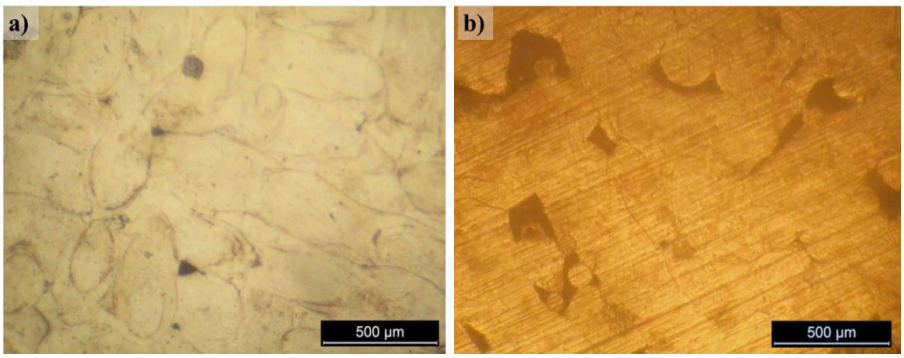

Figure 21. Vertically built specimens from experiment number: a) 8 (417 mm/s) and b) 46 (700 mm/s).

Higher scan spacing's can lead to poor sintering of adjacent regions of powder, not assuring a continuous bond between the consecutive lines of powders (like seen in Figure 22 a), where a high spacing value is used, contrasting with Figure 22 b)). This outcome leads to lower density and consequently lower mechanical properties.

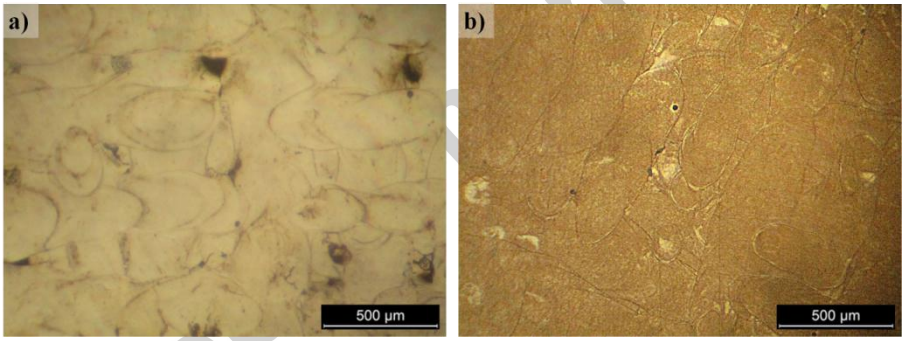

Figure 22. Vertically built specimens from experiment number: a) 12 (0.12 mm) and b) 15 (0.08 mm).

3.3. Effect of interaction between parameters

Horizontally built specimens

All the models obtained for shear strength, hardness and density showed that there are interactions between the independent variables (laser power (A); scan speed (B) and scan spacing (C)) (see Tables 4, 5 and 6). The effect of AC (laser power and scan spacing) was detected for shear strength (Figure 23 a)), for hardness (Figure 23 b)) and for density (Figure 23 c)). Additionally the effect of AB (laser power and scan speed) was also found for density (Figure 23 d)).

However, when analyzing Figure 23, it is possible to conclude that all these interaction effects are not expressive, once only minor variations on shear strength, on hardness and especially on density are observed for the given ranges of laser power, scan speed and scan spacing here tested and modelled.

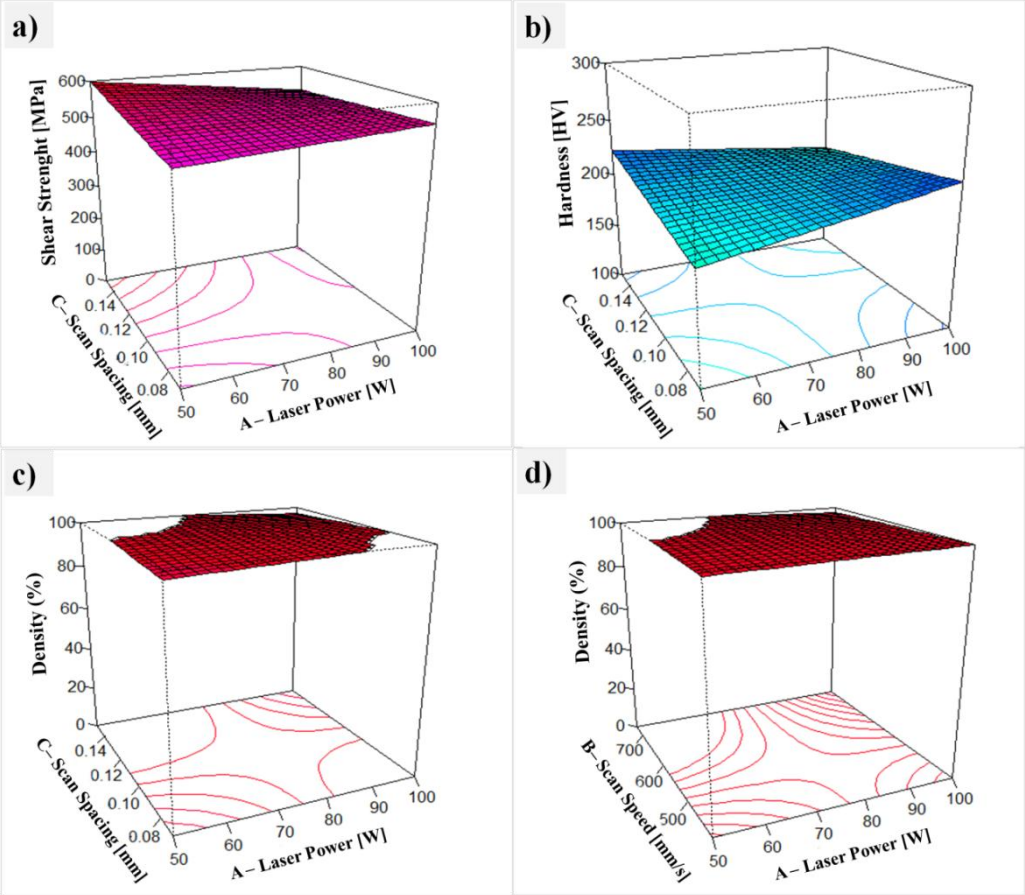

Figure 23. 3D response surface plots on: a) shear strength between laser power and scan spacing; b) hardness between laser power and scan spacing; c) density between laser power and scan spacing and d) density between laser power and scan speed for horizontally built specimens.

Vertically built specimens

All the models obtained for shear strength, hardness and density showed that there are interactions between the independent variables (laser power; scan speed and scan spacing) (see Tables 7, 8 and 9). The effect of AB (laser power and scan speed) was detected for shear strength, hardness and density (Figure 24 a), b) and e)). Additionally the effect of AC (laser power and scan spacing) was also found for hardness and density (Figure 24 c) and d)).

Figures 24 a) to e) show that for vertically built parts laser power and scan speed have a combined effect on shear strength, hardness and density.

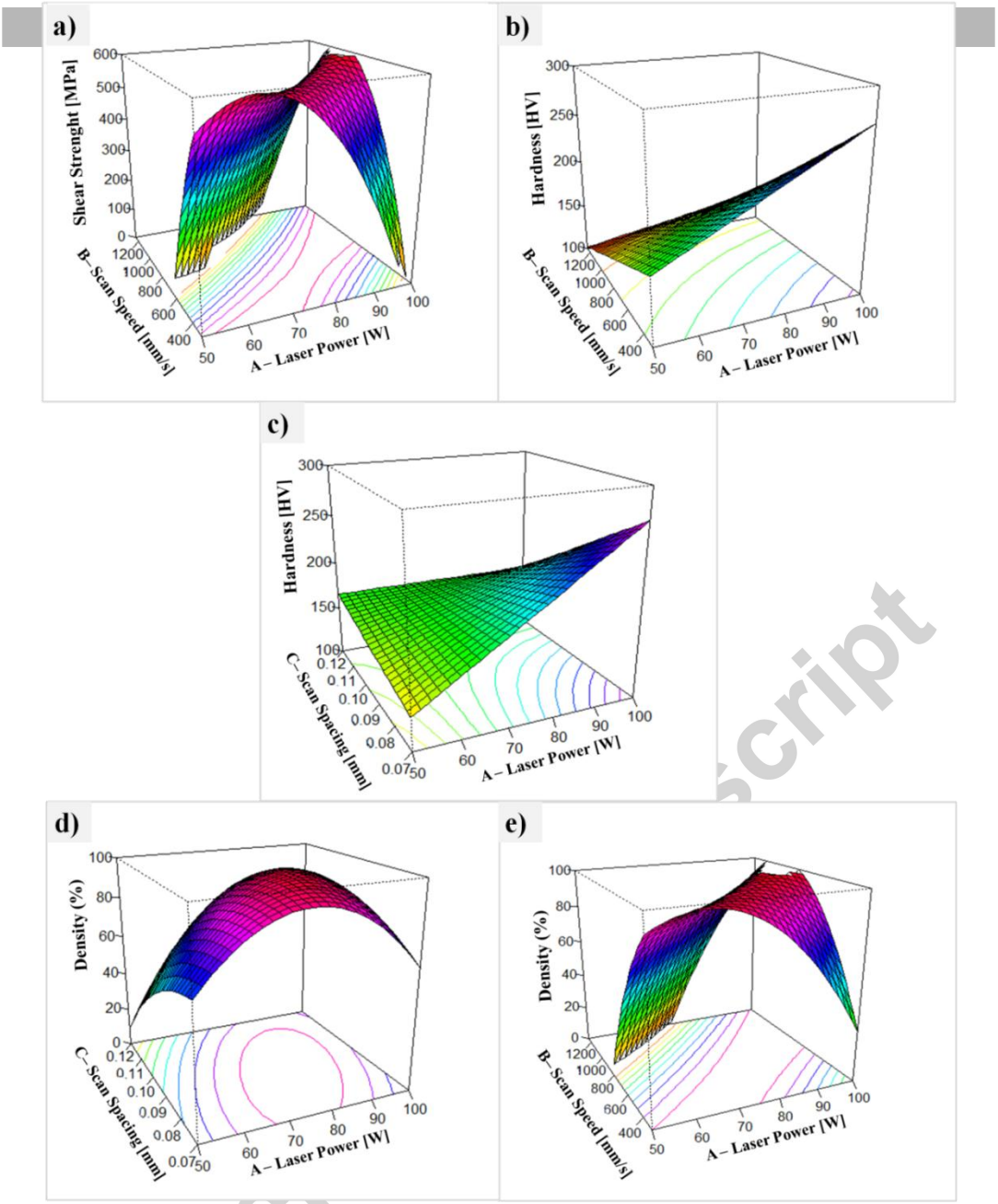

Figure 24. 3D response surface plots on (a) shear strength between laser power and scan speed; (b) hardness between laser power and scan speed; (c) hardness between laser power and scan spacing; (d) density between laser power and scan spacing and (e) density between laser power and scan speed for vertically built specimens.

When regarding hardness, Figure 24 b) shows that by increasing laser power, highest values are obtained, as for low, as for high scan speed values. Figure 24 c) shows that by increasing laser power, highest hardness values are attained, as for low, as for high scan spacing values. These results are correlated with the higher densification level and residual porosity progressive elimination when increasing the laser power.

When analyzing scan speed values, it is observable that for low scan speeds (situation where a high energy is applied per second in a given area, leading to good consolidation) the influence of the laser

power on hardness is very expressive (Figure 24 b)). On the other hand, for high scan speeds, the influence of laser power on hardness is not so expressive (Figure 24 b)), due to the highest percentage of consolidation defects that are obtained when using high scan speeds, which are not surpassed by increasing the laser power.

When analyzing scan spacing values, it is observable that for low scan spacing (situation where the highest consolidation is attained) the influence of the laser power on hardness is very expressive, once low scan spacing combined with high power lead to a great increase on the energy input on a given spot. Conversely, for high scan spacing's, the influence of laser power on hardness is not so expressive, once very high spacing leads to insufficient bond between adjacent layers of powder, drawback that is not solved by increasing the laser power.

Regarding shear strength, it is observable in Figure 24 a) that the highest value is obtained when using intermediate values of laser power and scan speed, thus obtaining an optimum compromise between these two parameters. Similarly, regarding density, the highest value is achieved when combining intermediate values of laser power and scan speed (as seen in Figure 24 e)) and also when combining intermediate values of laser power and scan spacing (as seen in Figure 24 d)). These findings for shear strength and density can be explained by the fact that by using extremely high energy, full densification it is unlikely to occur due to possible delamination of the sintered layers due to thermal stresses, balling effect, porosity due to gas pores formation and material shrinkage, as reported by Simchi [2].

3.4. Differences between horizontal and vertically built specimens

During SLM processing, the flow of heat from the laser beam occurs downwards (promoting bonding between the previous powder layer and the actual layer being processed) and also laterally (promoting bonding between adjacent regions of powder (scan lines) subjected to the laser beam. Due to this aspect, SLM 316L specimens exhibit anisotropic properties.

Owing to the different building strategy here tested, there are several differences between horizontal e vertically built specimens, namely: the numbers of built layers (more layers in horizontal specimens than in vertical ones); the solidification direction of the molten material (parallel to the specimen axes for vertical specimens and transversely for horizontal specimens), besides the supports number and position (necessary for the specimen growth).

Differences on density and mechanical properties of 316L specimens built by the two strategies here tested are clear when analyzing the six models here developed. Different influences of the three

process parameters here studied are visible when comparing vertical and horizontally built specimen's models. These differences can be related with the type, orientation and number of building defects which are acknowledged accountable for the density and mechanical properties reduction when using SLM technology, as reported by Chlebus [8]. Furthermore, once both types of specimens were tested for shear on the longitudinal plan, different aspects are being assessed: the bond between consecutive layers of powder on the case of horizontally built specimens and the bond between adjacent regions on any given layer.

4. Conclusions

- The broad objective of this work is to provide a deeper understanding on the influence of several SLM processing parameters (laser power, scan speed and scan spacing) on density, hardness and shear strength of 316L stainless steel. In this sense, predictive models were developed for each of these properties (dependent variable), using the aforesaid processing parameters as independent variables;
- The influence of the building orientation was studied by testing and developing predictive models for two different building strategies (horizontal and vertical);
- All the predictive models exhibit complex correlations of SLM process parameters, in most cases presenting a non-linear nature with multiple parameter interactions;
- Microstructural aspects of the produced parts were analyzed and correlated with the obtained predictive models;
- The developed models allow the prediction and optimization of 316L parts properties, produced by SLM.

Acknowledgements

This work was supported by the Portuguese Foundation of Science and Technology (FCT) through the projects EXCL/EMS-TEC/0460/2012, UID/EEA/04436/2013 and the grant SFRH/BPD/112111/2015.

References

[1] G. Casalino, S.L. Campanelli, N. Contuzzi, A.D. Ludovico, Experimental investigation and statistical optimisation of the selective laser melting process of a maraging steel, Opt. Laser. Technol. 65 (2015) 151-158.

[2] A. Simchi, Direct laser sintering of metal powders: Mechanism, kinetics and microstructural features, Mat. Sci. Eng. A-Struct. 428 (2006) 148-158.

[3] D. Gu, Y. Shen, Balling phenomena in direct laser sintering of stainless steel powder: Metallurgical mechanisms and control methods, Mater. Des. 30 (2009) 2903-2910.

[4] A. Simchi, F. Petzoldt, H. Pohl, On the development of direct metal laser sintering for rapid tooling, J. Mater. Process. Tech. 141 (2003) 319-328.

[5] E.O. Olakanmi, Selective laser sintering/melting (SLS/SLM) of pure Al, Al–Mg, and Al–Si powders: Effect of processing conditions and powder properties, J. Mater. Process. Tech. 213(2013) 1387-1405.

[6] E. Sallica-Leva, A.L. Jardini, J.B. Fogagnolo, Microstructure and mechanical behavior of porous Ti–6Al–4V parts obtained by selective laser melting, J. Mech. Behav. Biomed. 26 (2013) 98-108.

[7] J.P. Kruth, L. Froyen, J. Van Vaerenbergh, P. Mercelis, M. Rombouts, B. Lauwers, Selective laser melting of iron-based powder, J. Mater. Process. Tech. 149 (2004) 616–622.

[8] E. Chlebus, B. Kuźnicka, T. Kurzynowski, B. Dybała, Microstructure and mechanical behaviour of Ti—6Al—7Nb alloy produced by selective laser melting, Mater. Charact. 62 (2011) 488-495.

[9] R. Wauthle, B. Vrancken, B. Beynaerts, K. Jorissen, J. Schrooten, J.-P. Kruth, J. Van Humbeeck, Effects of build orientation and heat treatment on the microstructure and mechanical properties of selective laser melted Ti6Al4V lattice structures, Addit. Manuf. 5 (2015) 77–84.

[10] K. Antony, N. Arivazhagan, K. Senthilkumaran, Numerical and experimental investigations on laser melting of stainless steel 316L metal powders, J. Manuf. Process. 16 (2014) 345-355.

[11] C. Yan, L. Hao, A. Hussein, P. Young, D. Raymont, Advanced lightweight 316L stainless steel cellular lattice structures fabricated via selective laser melting, Mater. Des. 55 (2014) 533–541.

[12] A. Riemer, S. Leuders, M. Thöne, H.A. Richard, T. Tröster, T. Niendorf, On the fatigue crack growth behavior in 316L stainless steel manufactured by selective laser melting, Eng. Fract. Mech. 120 (2014) 15-25.

[13] R. Li, Y. Shi, Z. Wang, L. Wang, J. Liu, W. Jiang, Densification behavior of gas and water atomized 316L stainless steel powder during selective laser melting, Appl. Surf. Sci. 256 (2010) 4350–4356.

[14] L. Hao, S. Dadbakhsh, O. Seaman, M. Felstead, Selective laser melting of a stainless steel and hydroxyapatite composite for load-bearing implant development, J. Mater. Process. Tech. 209 (2009) 5793–5801.

[15] Q. Wei, S. Li, C. Han, W. Li, L. Cheng, L. Hao, Y. Shi, Selective laser melting of stainless-steel/nano-hydroxyapatite composites for medical applications: Microstructure, element distribution, crack and mechanical properties, J. Mater. Process. Tech. 222 (2015) 444-453.

[16] B. Dev, M.E. Walter, Comparative Study of the Leak Characteristics of Two Ceramic/Glass Composite Seals for Solid Oxide Fuel Cells, Fuel Cells (2014) DOI: 10.1002/fuce.201400095.

[17] Z.C. Du, J.G. Yang, Z.Q. Yao, B.Y. Xue, Modeling Approach of Regression Orthogonal Experiment Design for the Thermal Error Compensation of a CNC Turning Center, J. Mater. Process. Tech. 129 (2002) 619-623.

[18] C. S. Cheng, Projection Properties of Factorial Designs for Factor Screening, Springer, NewYork, 2006, pp. 156-168.

[19] R.K. Roy, Design of experiments using the Taguchi Approach, Wiley-Interscience Publication, John Wiley & Sons, Inc., 2001.

[20] J. Sander, J. Hufenbach, L. Giebeler, H. Wendrock, U. Kuhn, J. Eckert, Microstructure and properties of FeCrMoVC tool steel produced by selective laser melting, Mater. Des. 89 (2015) 335-341.

[21] O. Carvalho, S. Madeira, M. Buciumeanu, D. Soares, F.S. Silva, G. Miranda, Pressure and sintering temperature influence on the interface reaction of SiCp/410L stainless steel composites, J. Compos. Mater. (2015) DOI: 10.1177/0021998315598851.